

Theoretical investigation of elliptical high-order harmonic generation from H_2^+ in two-color cross-linearly-polarized laser fields

Cai-Ping Zhang(张彩萍), Si-Hui Wang(王思慧), Yu-Zhi Chen(陈育之), Xin-Ru Du(杜欣茹), and Xiang-Yang Miao(苗向阳)

Citation: Chin. Phys. B, 2025, 34 (**8**): 083301. DOI: 10.1088/1674-1056/add00a
http://cpb.iphy.ac.cn; http://iopscience.iop.org/cpb

What follows is a list of articles you may be interested in

Tuning the laser-dressed attosecond transient absorption spectra of a singly excited helium state using a shaped attosecond pulse with a spectral minimum

Yong Fu(傅勇), Feier Xu(徐霏儿), and Cheng Jin(金成)
Chin. Phys. B, 2025, 34 (**6**): 063302. DOI: 10.1088/1674-1056/adc40c

Generating attosecond pulses with controllable polarization from cyclic H_3^{2+} molecules by bichromatic circular fields

Si-Qi Zhang(张思琪), Bing Zhang(张冰), Bo Yan(闫博), Xiang-Qian Jiang(姜向前), and Xiu-Dong Sun(孙秀冬)
Chin. Phys. B, 2024, 33 (**2**): 023301. DOI: 10.1088/1674-1056/ad062b

Effect of aggregation on thermally activated delayed fluorescence and ultralong organic phosphorescence: QM/MM study

Qun Zhang(张群), Xiaofei Wang(王晓菲), Zhimin Wu(吴智敏), Xiaofang Li(李小芳), Kai Zhang(张凯), Yuzhi Song(宋玉志), Jianzhong Fan(范建忠), Chuan-Kui Wang(王传奎), and Lili Lin(蔺丽丽)
Chin. Phys. B, 2023, 32 (**10**): 103301. DOI: 10.1088/1674-1056/acb75d

A simple semiempirical model for the static polarizability of ions

Alexander S Sharipov and Boris I Loukhovitski
Chin. Phys. B, 2023, 32 (**8**): 083301. DOI: 10.1088/1674-1056/acd2b2

Decoding the electron dynamics in high-order harmonic generation from asymmetric molecular ions in elliptically polarized laser fields

Cai-Ping Zhang(张彩萍) and Xiang-Yang Miao(苗向阳)
Chin. Phys. B, 2022, 31 (**4**): 043301. DOI: 10.1088/1674-1056/ac29b0

Theoretical investigation of elliptical high-order harmonic generation from H_2^+ in two-color cross-linearly-polarized laser fields

Cai-Ping Zhang(张彩萍)[1,2], Si-Hui Wang(王思慧)[1,2], Yu-Zhi Chen(陈育之)[1,2], Xin-Ru Du(杜欣茹)[1,2], and Xiang-Yang Miao(苗向阳)[1,2,†]

[1] *College of Physics and Information Engineering, Shanxi Normal University, Taiyuan* 030031, *China*
[2] *Key Laboratory of Spectral Measurement and Analysis of Shanxi Province, Shanxi Normal University, Taiyuan* 030031, *China*

(Received 14 February 2025; revised manuscript received 31 March 2025; accepted manuscript online 24 April 2025)

We theoretically investigate the elliptical high-order harmonic generation from H_2^+ in two-color cross-linearly-polarized laser fields by numerically solving the two-dimensional time-dependent Schrödinger equation. Numerical simulations show that the crossing-angle-dependent harmonic ellipticity exhibits a prominent antisymmetric structure, which tends to disappear as the internuclear distance increases. Furthermore, ground-state electrons experience resonant transitions to the first excited state at larger internuclear distances, where the disruption of symmetric electron motion suppresses the antisymmetric structure. Additionally, a near-circularly-polarized attosecond pulse can be obtained by modulating the crossing angle.

Keywords: harmonic ellipticity, molecular ions, excited state, attosecond pulse

PACS: 33.80.Rv, 42.65.Ky, 42.65.Re

DOI: 10.1088/1674-1056/add00a **CSTR:** 32038.14.CPB.add00a

1. Introduction

High-order harmonic generation (HHG) is an interesting nonlinear phenomenon in strong field physics.[1–6] The dynamical process can be explained by three-step model.[7] Firstly, the electron is tunneling ionized, and then the ionized electron is accelerated in the external field. Finally, the electron recombines with the parent ion and releases high-energy photons. The HHG can be employed to generate attosecond pulses,[8,9] detect the atomic and molecular structures,[10,11] monitor ultrafast electron motion,[12,13] track chemical reaction processes,[14] and so on. Moreover, the elliptical harmonics have attracted widespread interest,[15,16] due to its unique advantages such as chiral recognition of molecules,[17] measurement of magnetic circular dichroism.[18]

For several decades, numerous methods have been proposed to generate elliptically polarized harmonics.[19–26] Kfir *et al.*[19] pointed that the elliptically polarized harmonics could be emitted when the atoms are irradiated by the bichromatic counter-rotating circularly polarized laser pulses. Moreover, the related harmonic intensity is comparable to that generated in the linearly polarized laser field. Dorney *et al.*[20] demonstrated that both the right-handed and left-handed polarized harmonic intensities can be enhanced by adjusting the relative intensity ratio of the bichromatic circularly polarized driving laser field. It results in the generation of the elliptically polarized attosecond pulses with ellipticity of 0.64. Huang *et al.*[21] found a linear relationship between the ellipticity of the harmonic emission and the ellipticity of the bichromatic counter-rotating driving pulses. And the polarization of harmonics can be modulated from linearly to circularly polarized. Chang *et al.*[22] controlled the polarization of harmonics via a transient nonlinear dipole grating. Li *et al.*[23] reported that the corotating bicircular laser fields were superior to the counter-rotating configurations in the harmonic generation with larger ellipticity. Furthermore, elliptically polarized attosecond pulses with the ellipticity of 0.88 were obtained by optimizing the frequency ratio. Son *et al.*[24] proved that the larger ellipticity arises from molecular orbital symmetry and two-center interference effect based on the high-precision calculations and analyses of the harmonics from H_2^+ with arbitrary orientation. Xing *et al.*[25] showed that the near-circularly polarized harmonics can be generated from the ring-current state of the Ne atoms in the two-color orthogonally polarized laser field by adjusting the intensity ratio. Sun *et al.*[26] revealed that the efficiency and polarization characteristics of the harmonics are closely related to the molecular alignment angle and the ellipticity of the driving laser field.

The laser-field parameter plays a crucial role in controlling the harmonic emission, making it advantageous to utilize as many parameters as possible. Notably, the two-color cross-linearly-polarized laser field encompasses a variety of adjustable parameters, including intensity, wavelength, crossing angle as well as relative phase. These parameters could provide multiple degree of freedoms for optimizing the harmonic generation. In recent years, the two-color cross-linearly-polarized laser fields were employed to generate el-

†Corresponding author. E-mail: sxxymiao@126.com

© 2025 Chinese Physical Society and IOP Publishing Ltd. All rights, including for text and data mining, AI training, and similar technologies, are reserved.

liptically polarized harmonics.[27–29] The crossing angle and the relative phase attracted much more attention in the geometry of the two-color cross-linearly-polarized laser field. Habibović *et al.*[27] regulated the intensity and the ellipticity of harmonics from Ne atoms by changing the frequency ratio and crossing angle of the two incident laser beams. In addition to investigating the impact of crossing angle on atomic harmonic generation,[28–30] Fang *et al.*[31] delved into the influence of relative phase on harmonics from He atoms. And the harmonic ellipticity was attributed to the different contributions of multiple quantum orbits. Compared with atomic systems, molecular systems offer additional degrees of freedom, enabling richer electron dynamics encoded in harmonics. Moreover, these dynamics are significantly modulated by the internuclear distance. However, the underlying physical dynamics and the polarization characteristics of harmonics from molecular ions remain unclear in two-color cross-linearly-polarized laser fields. Therefore, it is essential to further investigate the harmonic emission from molecular ions with varying internuclear distances.

In this work, the H_2^+ is employed to investigate the properties of the elliptical harmonics in two-color cross-linearly-polarized laser fields. As demonstrated in previous studies about the atomic harmonic emission,[28–31] the crossing angle remains an important parameter in molecular harmonic emission. Moreover, the results indicate that the crossing-angle-dependent harmonic ellipticity is sensitive to the internuclear distance. The obvious antisymmetric structure diminishes as the internuclear distance increases. Nevertheless, the harmonic ellipticity will be enhanced. This feature can be predominantly ascribed to the disruption of symmetric electron motion at larger internuclear distance. The underlying physical mechanism can be revealed via the electron population, time-resolved harmonic ellipticity and electron probability density distribution. Finally, an isolated near-circularly polarized attosecond pulse can be obtained from molecular harmonics emitted in the two-color cross-linearly-polarized laser field.

2. Theoretical method

By solving the two-dimensional TDSE, the elliptical harmonic emission from H_2^+ in the two-color cross-linearly-polarized laser field has been investigated. The TDSE can be written as

$$\mathrm{i}\frac{\partial}{\partial t}\psi(x,y,t) = \left[\frac{\hat{P}_x{}^2}{2\mu}+\frac{\hat{P}_y{}^2}{2\mu}+\hat{V}_{\mathrm{c}}(x,y) + xE_x(t)+yE_y(t)\right]\psi(x,y,t), \quad (1)$$

here $V_{\mathrm{c}}(x,y)$ is the soft-core Coulomb potential with the expression as follows:

$$V_{\mathrm{c}}(x,y) = -\frac{1}{\sqrt{(x-R/2)^2+y^2+a^2}} - \frac{1}{\sqrt{(x+R/2)^2+y^2+a^2}}, \quad (2)$$

where R is the internuclear distance. The soft-core parameter $a = 0.735$ is adopted to match the ionization potential $I_{\mathrm{p}} = 1.09$ a.u. (atomic unit) of the ground state at $R = 2$ a.u.[32] For the two-color cross-linearly-polarized laser field, one is polarized along the y direction and the other one forms a crossing angle θ with the y direction, expressed as

$$\begin{aligned} E_x(t) &= E_2 f(t)\sin(\theta)\cos(2\omega t-\varphi),\\ E_y(t) &= E_1 f(t)\cos(\omega t)+E_2 f(t)\cos(\theta)\cos(2\omega t-\varphi), \end{aligned} \quad (3)$$

here E_i $(i = 1,2)$ is the peak amplitude of the electric field. $f(t)$ is a five-optical-cycle (o.c.) trapezoidal envelope with one cycle ramp on, three cycles constant and one cycle ramp off. $\omega = 0.04558$ a.u. is the laser frequency, and $\varphi = 95^\circ$ is the relative phase. The time-dependent wave-function $\psi(x,y,t)$ is obtained via second-order split operator method.[33–36] The time step is 0.05 a.u. The spatial grid ranges from -200 a.u. to 200 a.u. in x direction and from -100 a.u. to 100 a.u. in the y direction, with 999 and 499 points, respectively. Namely, $\Delta x = \Delta y = 0.4$ a.u. The dipole acceleration is given by the Ehrenfest theorem,[37]

$$\begin{aligned} a_x(t) &= \langle\psi(x,y,t)\,|\,-\frac{\partial V(x,y)}{\partial x}+E_x(t)\,|\,\psi(x,y,t)\rangle,\\ a_y(t) &= \langle\psi(x,y,t)\,|\,-\frac{\partial V(x,y)}{\partial y}+E_y(t)\,|\,\psi(x,y,t)\rangle. \end{aligned} \quad (4)$$

The x and y components of harmonics ($P_x(\omega)$, $P_y(\omega)$) can be calculated by the Fourier transformation of dipole acceleration

$$\begin{aligned} P_x(\omega) &= \left|\frac{1}{\sqrt{2\pi}}\int a_x(t)\,\mathrm{e}^{-\mathrm{i}\omega t}\,\mathrm{d}t\right|^2,\\ P_y(\omega) &= \left|\frac{1}{\sqrt{2\pi}}\int a_y(t)\,\mathrm{e}^{-\mathrm{i}\omega t}\,\mathrm{d}t\right|^2. \end{aligned} \quad (5)$$

The time-resolved harmonics $H_{\mathrm{q}}(t)$ can be given via the wavelet transform of dipole acceleration.[31] The harmonic ellipticity can be expressed as[38]

$$\varepsilon = \frac{(|b_+|-|b_-|)}{(|b_+|+|b_-|)}, \quad (6)$$

where $b_\pm = \frac{1}{\sqrt{2}}(b_x \pm \mathrm{i}b_y)$, with b_x and b_y being the x and y components of dipole acceleration in frequency domain, respectively. Based on the $H_{\mathrm{q}}(t)$, the time-resolved harmonic ellipticity $\varepsilon'_{\mathrm{q}}(t)$ can also be obtained by Eq. (6). Additionally, the ellipticity can also be written as[24]

$$\varepsilon = \sqrt{\frac{1+r^2-\sqrt{1+r^4+2r^2\cos 2\delta}}{1+r^2+\sqrt{1+r^4+2r^2\cos 2\delta}}}, \quad (7)$$

here $r = |b_x(\omega)/b_y(\omega)|$ and $b_{x,y}(\omega) = \int_{-\infty}^{+\infty} a_{x,y}(t)\,\mathrm{e}^{-\mathrm{i}\omega t}\,\mathrm{d}t$. $\delta = \varphi_y(\omega)-\varphi_x(\omega)$ is the phase difference between x and y components of harmonics, and $\varphi_{x,y}(\omega) = \arg[a_{x,y}(\omega)]$. The

attosecond pulse can be generated by superposing harmonics in platform region,

$$I_{x,y}(t) = \left| \sum_{\mathrm{q}} b_{x,y}(q)\, \mathrm{e}^{\mathrm{i}q\omega t} \right|^2, \tag{8}$$

where q is the harmonic order.

3. Results and discussion

In numerical simulation, the H_2^+ is selected to investigate the properties of elliptical harmonics in the two-color cross-linearly-polarized laser field, as expressed in Eq. (3). Figure 1(a) shows the harmonic ellipticities for different R. Here, the crossing angle θ is equal to 90°. The peak intensity is $I_1 = I_2 = 2.0 \times 10^{14}$ W/cm^2 ($E_1 = E_2 = 0.075$ a.u.) unless otherwise stated. One can notice that the harmonic ellipticity is significantly sensitive to R. The ellipticity is about zero for the case of $R < 3.8$ a.u., and then becomes higher for larger R. When the internuclear distance increases to $R = 4.3$ a.u., the ellipticity is 0.96 for 25th order harmonic. So the crossing angle can dramatically affect the ellipticity of molecular harmonics. In order to get deep understanding about the influence of crossing angle, figures 1(b) and 1(c) depict the harmonic ellipticity as a function of crossing angle at $R = 2.0$ a.u. and $R = 4.3$ a.u., respectively. Astonishingly, the crossing-angle-dependent harmonic ellipticity is antisymmetric about $\theta = 90°$ at $R = 2.0$ a.u. in Fig. 1(b). However, this antisymmetric character is suppressed at $R = 4.3$ a.u., as demonstrated in Fig. 1(c). Additionally, the suppression of antisymmetric character can also be observed at larger internuclear distances, such as $R = 7.0$ a.u. and $R = 10.0$ a.u., where charge-resonance-enhanced ionization is typically expected to occur. The relative phase influences the value of harmonic ellipticity, but its effect on the symmetry of the structure in crossing-angle-dependent harmonic ellipticity could be neglected. Moreover, for the case of $\varphi = 95°$, harmonics from the 17th to 31st orders exhibit positive ellipticity at $R = 4.3$ a.u. and $\theta = 90°$, with some harmonics achieving values exceeding 0.8. This feature enhances the feasibility of generating attosecond pulse with higher ellipticity. Therefore, we primarily concentrate on the results at $\varphi = 95°$ in the subsequent discussion.

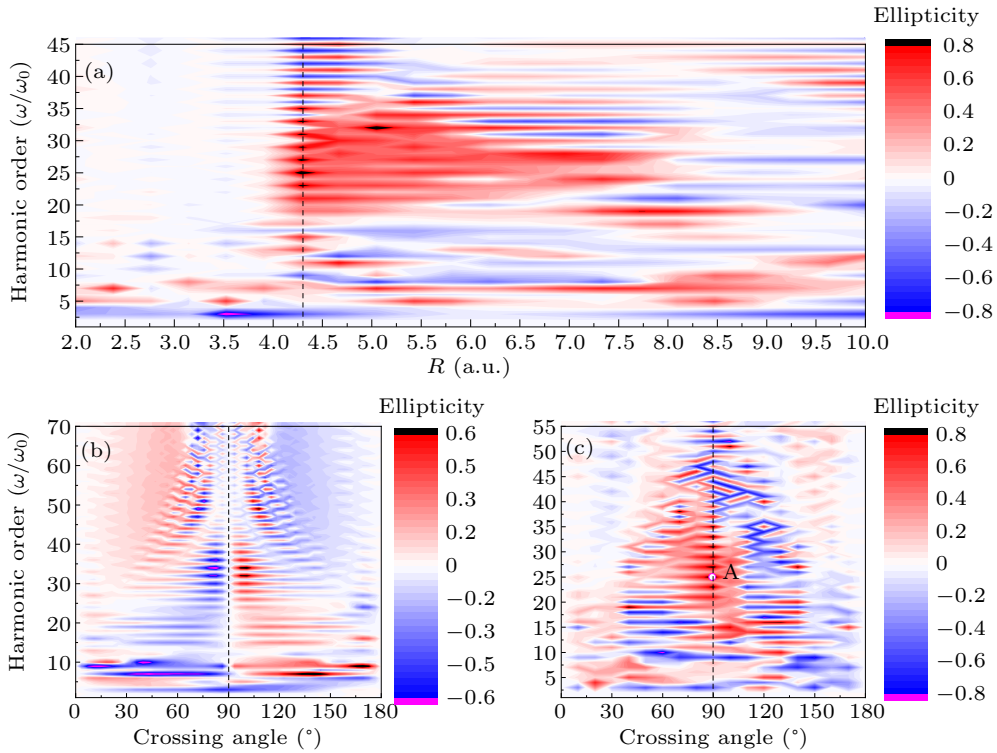


Fig. 1. (a) Harmonic ellipticities of H_2^+ from $R = 2.0$ a.u. to $R = 10.0$ a.u. at crossing angle $\theta = 90°$. (b)–(c) Crossing-angle-dependent harmonic ellipticities at $R = 2.0$ a.u. and $R = 4.3$ a.u., respectively.

To investigate the underlying electron dynamics in antisymmetric structure of crossing-angle-dependent harmonic ellipticity at $R = 2.0$ a.u., figures 2(a1)–2(c1) present the time-resolved harmonic ellipticity $\varepsilon'_{\mathrm{q}}(t)$ (pink shading) and harmonic intensity $H_{\mathrm{q}}(t)$ (blue line) for the 32nd order harmonic in one optical cycle at $\theta = 80°$, $\theta = 90°$, and $\theta = 100°$, respectively. Obviously, two harmonic bursts contribute to the 32nd order harmonic in one optical cycle. For the case of $\theta = 80°$ in Fig. 2(a1), the time-resolved ellipticity for harmonic burst A_1 is much smaller than that of B_1. After the time accumulation, the ellipticity of the 32nd order harmonic, dominated by B_1, is negative. When the crossing angle increases to $\theta = 90°$ in Fig. 2(b1), harmonic bursts A_2 and B_2 exhibit identical intensities but opposite helicities; consequently, the ellipticity of the 32nd harmonic approaches zero. In Fig. 2(c1), the ellipticity at $\theta = 100°$ is dominated by A_3, resulting in a posi-

tive value. Because harmonic emission is intrinsically linked to electron distributions, the populations of electrons in the ground state and the first excited state at $R = 2.0$ a.u. are illustrated in Figs. 2(a2)–2(c2). It can be seen that electrons mainly locate in ground state, and undergo gradual variation induced by external laser field. Consequently, at $R = 2.0$ a.u., harmonic emission is dominated by electrons in the ground state. Moreover, the harmonic intensity is mainly determined by electric field along x-direction, which is parallel to the molecular axis. According to Eq. (3), the amplitude of E_x ($\theta = 80°$) is equal to that of E_x ($\theta = 100°$), which results in nearly identical harmonic intensities at these symmetric crossing angles as blue lines depicted in Figs. 2(a1) and 2(c1). To further understand the mechanism of opposite helicities at $\theta = 80°$ and $\theta = 100°$, electron probability density distributions in the x and y directions are demonstrated in Figs. 3(a)–3(d). Under the influence of laser field, only electrons recombining with nucleus simultaneously in both the x and y directions, could contribute to harmonic emission. Due to the periodicity of electron motion, we present electron probability density distributions from 2 o.c. to 3 o.c. in Figs. 3(a)–3(d). As shown by dash lines in Figs. 3(a) and 3(b), the elliptical harmonics at $\theta = 80°$ primarily originate from the electron distribution in the second half-cycle, whereas those at $\theta = 100°$ arise from the electron distribution in the first half-cycle, as illustrated in Figs. 3(c) and 3(d). The elliptical harmonics at $\theta = 100°$ are generated a half cycle earlier than those at $\theta = 80°$. In other words, the phase difference between harmonics at $\theta = 100°$ and $\theta = 80°$ is equal to π. Therefore, the harmonic helicities are opposite for crossing angles symmetric about $\theta = 90°$ at $R = 2.0$ a.u.

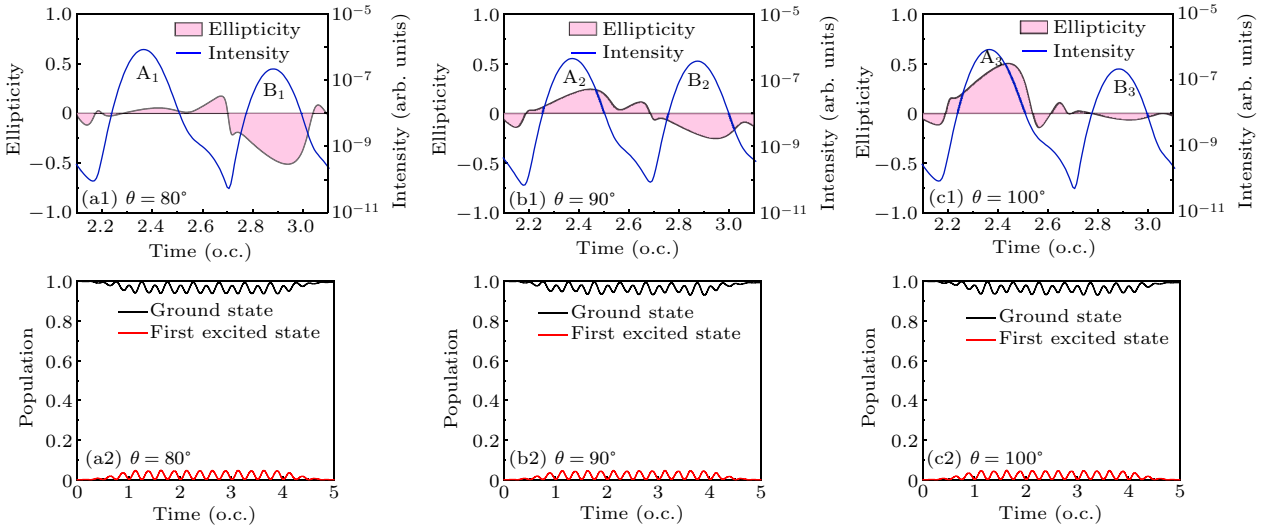


Fig. 2. (a1)–(c1) Temporal distributions of the 32nd order harmonic's ellipticity (pink shading) and intensity (blue line) in one optical cycle at different crossing angles (a) $\theta = 80°$, (b) $\theta = 90°$, and (c) $\theta = 100°$, respectively. (a2)–(c2) Populations of electrons in the ground state and the first excited state. Here R is 2.0 a.u.

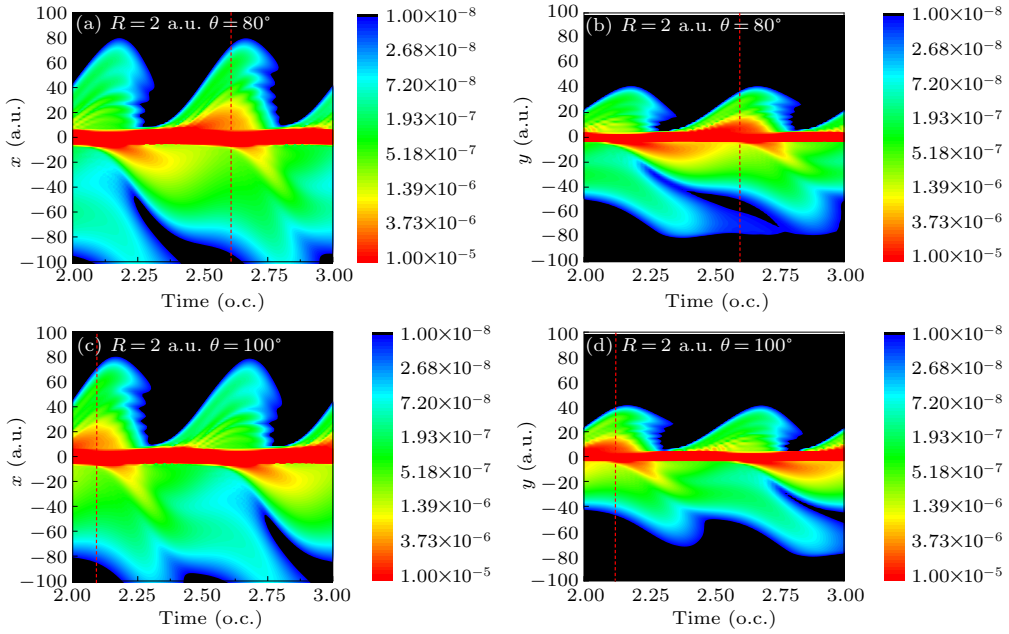


Fig. 3. Electron probability density distributions in the x and y directions at $R = 2.0$ a.u. for different crossing angles: (a)–(b) $\theta = 80°$, and (c)–(d) $\theta = 100°$.

Unlike the results at $R = 2.0$ a.u. as shown in Fig. 1(b), the antisymmetric structure is significantly suppressed at $R = 4.3$ a.u. Additionally, the ellipticities of certain harmonics at $\theta = 90^\circ$ are markedly enhanced. For instance, the 25th-order harmonic demonstrates an ellipticity of 0.96 at point A in Fig. 1(c). What accounts for the distinct difference in crossing-angle-dependent ellipticity structures between large and small internuclear distances? It is well known that the coupling between the ground state and the first excited state becomes stronger as R increases, thereby facilitating the electron transition between these two states. To elucidate the differences in the crossing-angle-dependent ellipticity structures between $R = 2.0$ a.u. and $R = 4.3$ a.u. in Fig. 1, the populations of electrons in the ground state and the first excited state at $R = 2.0$ a.u. (red line) and $R = 4.3$ a.u. (black line) for $\theta = 90^\circ$ are demonstrated in Figs. 4(a) and 4(b), respectively. At $R = 2.0$ a.u., the energy difference between the ground state and the first excited state is 0.42 a.u. Owing to this considerable energy gap, electron transition between these two electronic states is significantly suppressed. As depicted in Figs. 4(a) and 4(b), the population of electrons in the ground state (red line) is greatly higher than that of the first excited state at $R = 2$ a.u. Consequently, the electron transition at $R = 2.0$ a.u. has negligible impact on the harmonic ellipticity. The energy gap between the ground state and the first excited state decreases with the increasing of R. At $R = 4.3$ a.u., the energy gap approaches twice the photon energy of the fundamental field ($\omega = 0.04558$ a.u.). Therefore, the resonant transition from the ground state to the first excited state occurs via two-photon absorption, leading to a notable increase in the population of electrons in the first excited state (black line) as shown in Fig. 4(b). On the one hand, electrons in the first excited state could be easily ionized, resulting in harmonic intensities of P_x and P_y at $R = 4.3$ a.u. approximately three orders magnitude higher than those at $R = 2.0$ a.u., as depicted in Fig. 4(c). Additionally, the intensities of P_x and P_y are comparable at $R = 4.3$ a.u. On the other hand, the first excited state also affects the harmonic phase. In Fig. 4(d), the phase difference between the x and y components remains around 0 π or $\pm\pi$ at $R = 2.0$ a.u., which dominated by electrons in the ground state. However, the phase difference between the x and y components shifts around $\pm 0.5\pi$ from 17th to 31st order harmonics at $R = 4.3$ a.u. For the 25th order harmonic at $R = 4.3$ a.u., the intensity ratio between the x and y components is 1.06, and the related phase difference is 0.5 π. Based on Eq. (7), the 25th-order harmonic is near-circularly polarized. In a word, the resonant transition from the ground state to the first excited state plays an important role in harmonic ellipticity at $R = 4.3$ a.u. and $\theta = 90^\circ$.

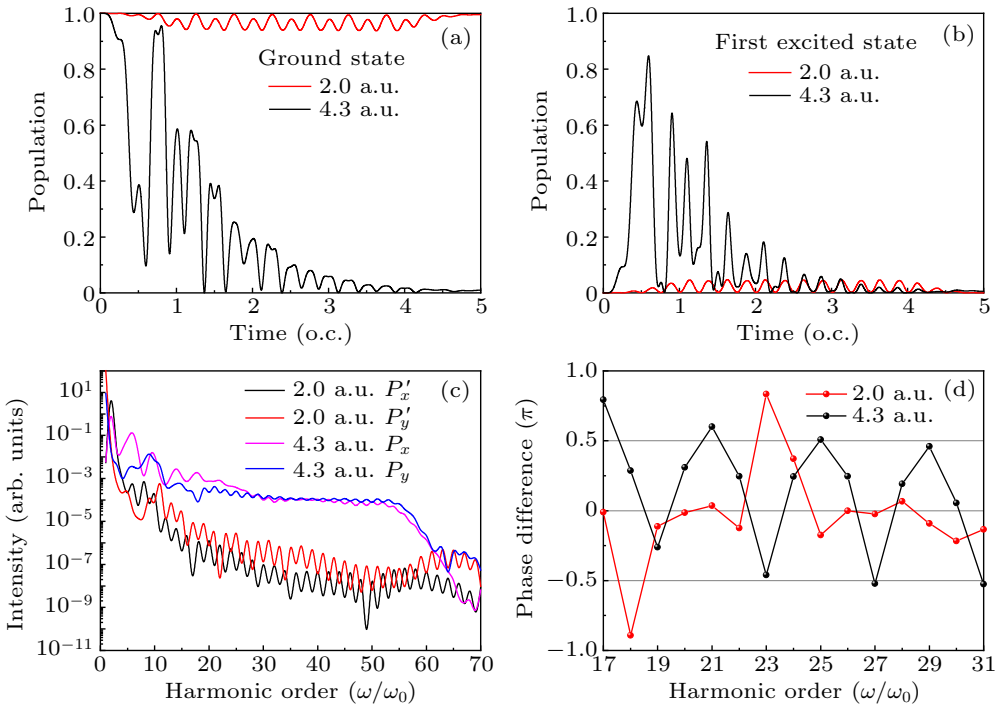


Fig. 4. (a)–(b) Populations of electrons in the ground and first excited states at $R = 2.0$ a.u. (red line) and $R = 4.3$ a.u. (black line), respectively. (c) The x and y components of harmonic spectra at $R = 2.0$ a.u. (P_x', P_y') and $R = 4.3$ a.u. (P_x, P_y), respectively. (d) Phase difference between x and y components of harmonics from the 17th to 31st orders at $R = 2.0$ a.u. and $R = 4.3$ a.u., respectively. All results are under the condition of $\theta = 90^\circ$.

To elucidate the physical mechanism of the antisymmetric structure suppression at $R = 4.3$ a.u., electron dynamics of harmonic emissions at $\theta = 80^\circ$ and $\theta = 100^\circ$ are investigated. In Fig. 5(a), ellipticities of harmonics from 19th to 30th orders are positive both at $\theta = 80^\circ$ and $\theta = 100^\circ$, indicating a lack of antisymmetric characteristics. As above mentioned, the resonant transition from the ground state to the first excited state significantly affects the harmonic ellipticity at $R = 4.3$ a.u. and

$\theta = 90°$. In Fig. 5(b), we provide the populations of electrons in the first excited state at $\theta = 80°$ (black line) and $\theta = 100°$ (red line), respectively. It can be seen that the population of electrons in the first excited state at $\theta = 80°$ is similar to that at $\theta = 100°$, which is attributed to the resonant transition via two-photon absorption. A great number of electrons in the first excited state could considerably enhance the ionization process. Subsequently, these ionized electrons will be accelerated in the two-color cross-linearly-polarized laser field. Moreover, electron motion is affected by E_x and E_y. Based on Eq. (3), $E_x(\theta = 80°) = E_x(\theta = 100°)$, $E_y(\theta = 80°) \neq E_y(\theta = 100°)$. As expected, electron motion in the x direction at $\theta = 80°$ is similar to that at $\theta = 100°$ under the interaction of identical laser intensity in the x direction, as demonstrated by electron probability density distributions in Figs. 5(c) and 5(d). Since there are substantial ionized electrons at both $\theta = 80°$ and $\theta = 100°$, the effects of the laser intensity in y direction are amplified. As dash line shown in Figs. 5(e) and 5(f), electron motion in the y direction at $\theta = 80°$ differs from that at $\theta = 100°$. In other words, the symmetry of electron motion is disrupted due to E_y ($\theta = 80°$) $\neq E_y$ ($\theta = 100°$). In this case, the ionized electrons tend to recombine with parent ions via trajectories without symmetry. As a result, the antisymmetric structure in crossing-angle-dependent ellipticity is suppressed. Additionally, this mechanism can be verified by setting $E_1(t)$ along the x direction instead of the y direction. Specifically, $E_x'(t) = E_2 f(t)\sin(\theta)\cos(2\omega t - \varphi) + E_1 f(t)\cos(\omega t)$ and $E_y'(t) = E_2 f(t)\cos(\theta)\cos(2\omega t - \varphi)$. In this scenario, $E_x(\theta) = E_x(\pi - \theta)$ and $E_y(\theta) = -E_y(\pi - \theta)$. Moreover, the antisymmetric structure of the crossing-angle-dependent harmonic ellipticity is independent of R. Due to its similarity with the results in Fig. 1(b), the simulation results for the case of $E_1(t)$ along the x direction not presented here. Therefore, it is the disruption of the symmetric electron motion at $R = 4.3$ a.u. that suppresses the antisymmetric structure in crossing-angle-dependent harmonic ellipticity.

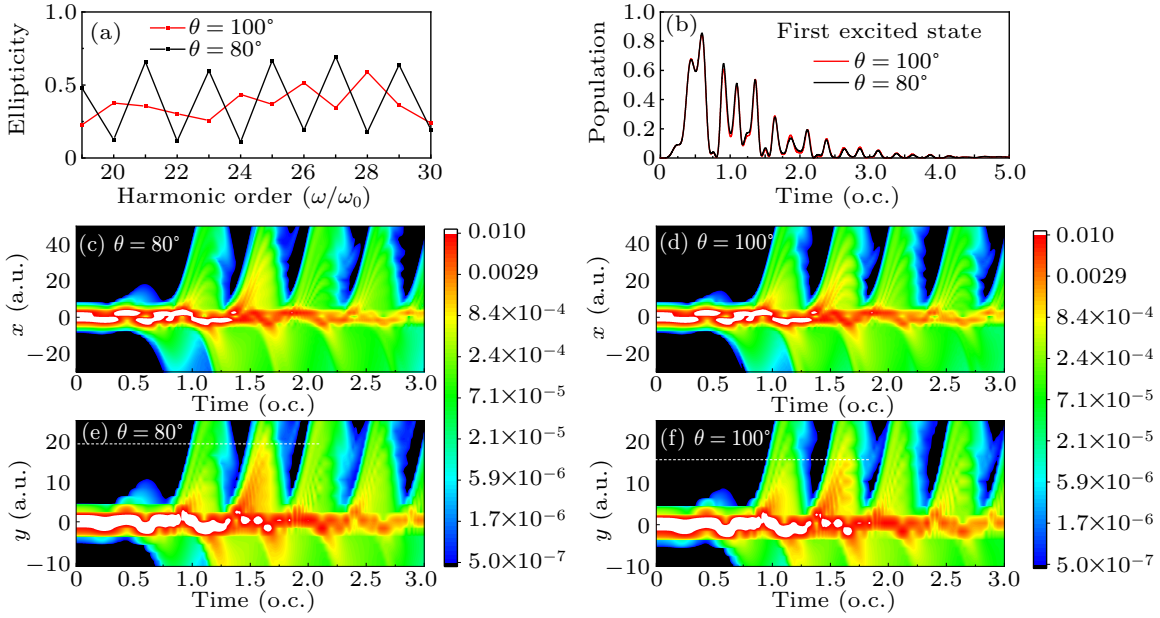


Fig. 5. (a) Harmonic ellipticity at $\theta = 80°$ and $\theta = 100°$, respectively. (b) Populations of electrons in the first excited state at $\theta = 80°$ (black line) and $\theta = 100°$ (red line), respectively. (c)–(f) Electron probability density distributions in the x and y directions at $\theta = 80°$ and $\theta = 100°$, respectively.

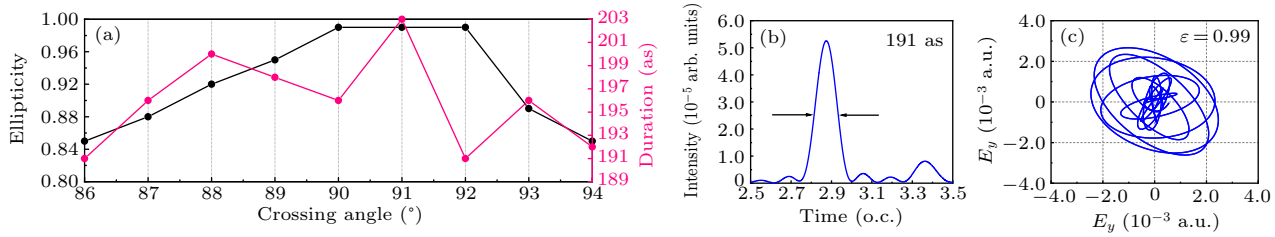


Fig. 6. (a) Crossing-angle-dependent ellipticity (black circles) and duration (pink circles) of the attosecond pulse. (b)–(c) Temporal profile and projection of the attosecond pulse on the x–y plane at $\theta = 92°$, respectively. Here, the superposed harmonics range from the 23rd order to the 30th order at $R = 4.3$ a.u.

The harmonic generation is viewed as an ideal source for generating attosecond pulses.[1,8,16] As can be seen from Fig. 1(c), the harmonic ellipticity is larger in the range from $\theta = 80°$ to $\theta = 100°$. So an isolate elliptically polarized attosecond pulse can be obtained by superposing several orders of harmonics at appropriate crossing angle. Figure 6(a) illustrates the crossing-angle-dependent ellipticity (black circles) and the duration (pink circles) of the attosecond pulse. The attosecond pulse is synthesized by superposing harmonics from the 23rd to the 30th orders at $R = 4.3$ a.u. Here, I_1 and I_2

are 2.0×10^{14} W/cm^2. It shows that both the duration and the ellipticity are sensitive to the crossing angle. Moreover, attosecond pulses with the maximum ellipticity of 0.99 could be generated at $\theta = 90°$, $\theta = 91°$, and $\theta = 92°$, respectively. As depicted in Fig. 6(b), the shortest duration is 191 as at $\theta = 92°$, and the projection of electric field of the attosecond pulse on the x–y plane is presented in Fig. 6(c). The results indicate that superposing harmonics from molecular ions in the two-color cross-linearly-polarized field is an effective method to generate near-circularly-polarized attosecond pulses.

4. Conclusion

In general, we have theoretically investigated the elliptical harmonics from H_2^+ in the two-color cross-linearly-polarized laser field by solving the two-dimensional time-dependent Schrödinger equation. The numerical results show that the crossing-angle-dependent harmonic ellipticity is antisymmetric about $\theta = 90°$ at $R = 2.0$ a.u. However, with the increase of internuclear distance, this antisymmetric structure tends to be suppressed. It reveals the significant role of the first excited state in elliptical harmonic emission by analyzing the harmonic ellipticities at different internuclear distances. Furthermore, an isolated attosecond pulse with the ellipticity of 0.99 can be obtained at $R = 4.3$ a.u. by adjusting the crossing angle. This work could provide an effective way to generate near-circularly-polarized attosecond pulses from aligned molecules.

Acknowledgements

Project supported by the National Natural Science Foundation of China (Grant Nos. 11974229, 12204291, and 11404204) and the Fund from Graduate Students of Shanxi Normal University, China (Grant No. 2023XSY044).

References

[1] Krausz F and Ivanov M 2009 *Rev. Mod. Phys.* **81** 163
[2] Qian C, Jiang S C, Wu T, Weng H M, Yu C and Lu R F 2024 *Phys. Rev. B* **109** 205401
[3] Hu C X and He F 2024 *Phys. Rev. A* **109** 033113
[4] Zhang Y P, Zhang M Y, Yang W L, Yu H Y, Xue S and Du H C 2023 *Phys. Rev. A* **108** 043508
[5] Zhang C P, Xia C L, Jia X F and Miao X Y 2016 *Opt. Express* **24** 20297
[6] Jin J Z, Liang H, Xiao X R, Wang M X, Chen S G, Wu X Y, Gong Q H and Peng L Y 2019 *Phys. Rev. Rev. A* **100** 013412
[7] Corkum P B 1993 *Phys. Rev. Lett.* **71** 1994
[8] Baltuška A, Udem T, Uiberacker M, Hentschel M, Goulielmakis E, Gohle C, Holzwarth R, Yakovlve V S, Scrinzi A, Hänsch T W and Krausz F 2003 *Nature* **421** 611
[9] Li J, Li K, Zhang X S, Popmintchev D, Xu H, Wang Y T, Li R X, Zhang G Y, Tang J Y, Niu J, Ma Y J, Meng R Y, Ke C J, Qiu J S, Ma Y F, Popmintchev T and Fan Z W 2024 *Light Sci. Appl.* **13** 12
[10] Itatani J, Levesque J, Zeidler D, Niikura H, Pépin J C, Corkum P B and Villeneuve D M 2004 *Nature* **432** 867
[11] Fu T T, Zhou S S, Chen J G, Wang J, Guo F M and Yang Y J 2023 *Opt. Express* **31** 30171
[12] Haessler S, Caillat J, Boutu W, Ruchon T, Auguste T, Breger P, Maquet A, Carré B, Taïeb R and Salières P 2010 *Nat. Phys.* **6** 200
[13] Shu Z, Liang H J, Wang Y C, Hu S L, Chen S, Xu H F, Ma R, Ding D J and Chen J 2022 *Phys. Rev. Lett.* **128** 183202
[14] Wörner H J, Bertrand J B, Kartashov D V, Corkum P B and Villeneuve D M 2010 *Nature* **466** 604
[15] Hu J, Wang Y C, Jing Q S, Jiang W, Wang G W, Zhao Y W, Xiao B, Liang H J and Ma R 2024 *Chin. Phys. B* **33** 054208
[16] Zhang X F and Zhu X S 2022 *Chin. Phys. B* **31** 114209
[17] Radu I, Vahaplar K, Stamm C, Kachel T, Pontius N, Dürr H A, Ostler T A, Evans J, Barker J, Evans R F L, Chantrell R W, Tsukamoto A, Kirilyuk A, Rasing T and Kimel A V 2011 *Nature* **472** 205
[18] Ferré A, Handschin C, Dumergue M, Burgy F, Comby A, Descamps D, Fabre B, Garcia G A, Géneaux R, Merceron L, Mével E, Nahon L, Petit S, Pons B, Staedter D, Ruchon T, Blanchet V and Mairesse Y 2015 *Nat. Photon.* **9** 93
[19] Kfir O, Grychtol P, Turgut E, Knut R, Zusin D, Popmintchev D, Popmintchev T, Nembach H, Shaw J M, Fleischer A, Kapteyn H, Murnane M and Cohen O 2015 *Nat. Photon.* **9** 99
[20] Dorney K M, Ellis J L, Hernández-García C, Hickstein D D, Mancuso C A, Brooks N, Fan T T, Fan G Y and Zusin D 2017 *Phys. Rev. Lett.* **119** 063201
[21] Huang P C, Hernández-García C, Huang J T, Huang P Y, Lu C H, Rego L, Hickstein D D, Ellis J L, Jaron-Becker A, Becker A, Yang S D, Durfee C G, Plaja L, Kapteyn H C, Murnane M M, Kung A H and Chen M C 2018 *Nat. Photon.* **12** 349
[22] Chang K Y, Huang L C, Asaga K, Tsai M S, Rego L, Huang P C, Mashiko H, Oguri K, Hernández-García C and Chen M C 2021 *Optica* **8** 484
[23] Li W Q, Zhu X S, Lan P F and Lu P X 2022 *Phys. Rev. A* **106** 043115
[24] Son S K, Telnov D A and Chu S I 2010 *Phys. Rev. A* **82** 043829
[25] Xing Y H, Zhang J, Huo X X, Lin S, Wang S, Li Z A and Liu X S 2024 *Phys. Rev. A* **109** 013111
[26] Sun F J, Chen C, Li W Y, Liu X, Li W and Chen Y J 2021 *Phys. Rev. A* **103** 053108
[27] Habibović D, Becker W and Milošević D B 2022 *Phys. Rev. A* **106** 023119
[28] Lambert G, Vodungbo B, Gautier J, Mahieu B, Malka V, Sebban S, Zeitoun P, Perron J, Andreev A, Stremoukhov S, Ardana-Lamas F, Dax A, Hauri C P, Sardinha A and Fajardo M 2015 *Nat. Commun.* **6** 6167
[29] Mahieu B, Stremoukhov S, Gauthier D, Spezzani C, Vodungbo B, Zeitoun P, Malka V and Ninno G D 2018 *Phys. Rev. A* **97** 043857
[30] Zhai C Y, Shao R Z, Lan P F, Wang B C, Zhang Y F, Yuan H, Njoroge S M, He L X and Lu P X 2020 *Phys. Rev. A* **101** 053407
[31] Fang Y Q and Liu Y Q 2021 *Phys. Rev. A* **103** 033116
[32] Li M Z, Xu Y, Jia G R and Bian X B 2019 *Phys. Rev. A* **100** 033410
[33] Lu R F, Zhang P Y and Han K L 2008 *Phys. Rev. E* **77** 066701
[34] Miao X Y and Zhang C P 2014 *Phys. Rev. A* **89** 033410
[35] Miao X Y and Du H N 2013 *Phys. Rev. A* **87** 053403
[36] Tong X M and Chu S I 2000 *Phys. Rev. A* **61** 021802
[37] Burnett K, Reed V C and Knight P L 1992 *Phys. Rev. A* **45** 3347
[38] Huo X X, Xing Y H, Qi T, Sun Y, Li B, Zhang J and Liu X S 2021 *Phys. Rev. A* **103** 053116